Evaluation of residual stress levels in plasma electrolytic oxidation coatings using a curvature method

J. Dean, T. Gu, T.W. Clyne *

Department of Materials Science and Metallurgy, Cambridge University, 27 Charles Babbage Road, Cambridge CB3 0FS, UK

ARTICLE INFO

ABSTRACT

Experimental estimates have been made of typical levels of residual stress in plasma electrolytic oxidation (PEO) coatings formed on aluminium and magnesium alloy substrates. This has been done via measurement of the curvature exhibited by thin strip samples, coated on one side only, using coating stiffness values obtained in the current work. In order to obtain curvatures that were sufficiently large to be accurately measurable, it was necessary to produce relatively thick (~100 μm) coatings on relatively thin (~300–500 μm) substrates. In such cases, stress levels are significant in both constituents, and there are significant through-thickness gradients of stress. The relevant characteristics of the transformation (largely oxidation of the substrate) are therefore best expressed as a misfit strain. This was found to have a magnitude of about 0.6–0.9 millistrain for the Al substrate and 2–3 millistrain for Mg, with a positive sign (so that the stress-free in-plane dimensions of the coating are larger than those of the residual substrate). This puts the coating into residual compression and, on a thick substrate, typical stress levels would be around 40–50 MPa for Al and 130–150 MPa for Mg. These values should be regarded as approximate, although their order of magnitude is probably reliable. They are higher than those from the (very limited) previous work carried out using this type of technique. On the other hand, they are lower than many values obtained using X-ray diffraction. Explanations are proposed for these discrepancies.

© 2014 The Authors. Published by Elsevier B.V. This is an open access article under the CC BY license (http://creativecommons.org/licenses/by/4.0/).

1. Introduction

Plasma electrolytic oxidation (PEO) coatings are formed by substrate oxidation in an aqueous electrolyte, via a series of localized electrical discharge events [1–3]. PEO coatings generated on aluminium generally contain a mixture of the α and γ phases of alumina, often with a significant amorphous content. When silicon is present, alumino-silicate phases such as mullite may also form [3–6]. The presence of substantial proportions of crystalline phases is probably responsible for the high hardness of PEO coatings on aluminium [3,4,7]. Local elastic moduli (obtained by nano-indentation) are usually also quite high (~100–400 GPa) [3,4,7]. However, the macroscopic stiffness (typically ~10–60 GPa) is sharply reduced by the presence of microcracks and porosity [3,5–12].

It might be expected that this low stiffness, combined with the fact that through-thickness plasma discharges cause restructuring of the coating throughout its growth, presumably relaxing residual stresses in their vicinity, would have the effect of ensuring that residual stresses in PEO coatings are relatively low. Certainly, this would be consistent with the common observation that PEO coatings do not readily debond from their substrates. Of course, the partial consumption of the substrate during coating growth would be expected to ensure that the interface was an intimate one, probably with a high toughness. Nevertheless, if there were high residual stresses in a PEO coating, then the associated stored elastic strain energy would constitute a strong driving force for spallation, particularly since PEO coatings are often relatively thick, and decohesion might then be expected within the coating (close to the interface), since the coating itself is unlikely to have a high fracture toughness. There have been very few direct measurements of the toughness of PEO coatings on Al substrates, but the information that is available [13,14] suggests that it tends to be relatively low ($G_c < $ ~few hundred J m^{-2}), and this is certainly consistent with expectations for a heavily micro-cracked and porous ceramic. Furthermore, there has been a study [15] of interfacial fracture in an Al alloy substrate/ PEO coating system, using the 4-point bending delamination test. The load-displacement data were not actually used to obtain an interfacial fracture energy value, but it was observed that there was a tendency for interfacial cracks to deviate into the coating, confirming that it has a lower toughness than the interface. There appears to be no information available concerning the toughness of PEO coatings on substrates other than Al.

Despite the significance of residual stress levels in PEO coatings, there is a substantial degree of uncertainty about them. There have been various experimental measurements [16–20] based on X-ray diffraction (peak shifts). Such publications commonly report wide

* Corresponding author. Tel.: +44 1223 334332.
  E-mail address: twc10@cam.ac.uk (T.W. Clyne).

ranges of stress magnitude, often up to very high levels (hundreds of MPa, and even into the GPa range in some cases) and in many cases apparently varying substantially as a consequence of changes in processing conditions, alloy composition, etc. Such high levels, and such variations, seem inherently unlikely in such compliant and relatively thick coatings. However, it is not really surprising that XRD tends to yield variable, and potentially unreliable, results for these coatings. The fact that, for alumina, two different phases are usually present (both of them with rather complex and variable crystal structures), that the crystallites are invariably very fine (giving considerable size broadening of the peaks) and that extraneous elements (from the electrolyte and/or the substrate) often get incorporated in the coating means that XRD data need to be interpreted with considerable care when used to infer residual stress levels in these coatings. For other substrates, such as Mg, similar arguments apply about the effects of a fine grain size, compositional variations, etc., even when there is only a single, well-defined crystal structure.

An alternative approach involves measurement of curvature induced by residual stresses in the coating when a relatively thin strip specimen has been coated on one side only. This technique has not been extensively applied to PEO coatings, but a similar approach was employed in a study recently published by Kuznetsov et al. [21] using Al-Mg alloy samples of thickness 200–500 µm, width 10 mm and length 160 mm. They created coating thicknesses of about 50 µm, obtained consistent, measurable curvatures and deduced that the coating stress was compressive in all cases, with a magnitude of around 10 MPa (and some dependence on process variables such as the average current). There are some concerns about their calculations, including their usage of a "theoretical" (fully dense) stiffness value for the coating (of 300 GPa), but it is clear that their measurements do indicate that the stress levels were appreciably lower than those from most X-ray diffraction studies.

In the present work, a similar curvature measurement method has been employed to evaluate residual stress levels created in representative PEO coatings (on Al and Mg). With this procedure, as with the work of Kuznetsov et al., the experimental outcome is not dependent on any assumptions relating to lattice strain, crystal structures, texture, etc., but is simply a function of the macroscopic elastic constants, the sample dimensions and the (misfit) strain associated with the transformation concerned, which in this case arises primarily from the conversion of Al or Mg to its oxide (albeit via a highly complex process). Consistent with these stresses being expected to be relatively low, and partly because of the difficulty of accurately measuring a very small curvature in a PEO system, it proved necessary to create relatively thick coatings on relatively thin substrates, and also to take certain steps when making the measurements and carrying out the analysis.

2. Experimental procedures

2.1. Sample preparation

Coatings were produced on Al-6082 and Mg-AZ31 substrates, in the form of sheet cut into relatively thin strips, with dimensions respectively of $100 \times 10 \times 0.3$ mm and $150 \times 10 \times 0.5$ mm. These samples were masked on all but one surface by casting (Epofix) resin around them. The resin held the samples rigidly during coating production, so that no curvature developed until they were released. This created boundary conditions consistent with the analysis being applied (see §4.2 and §4.3). Coatings were prepared using a 10 kW Keronite™ processing rig and an electrolyte consisting primarily of a dilute aqueous solution of KOH and Na_2SiO_4 for Al and a proprietary silicate-based electrolyte for Mg. The electrolyte was maintained at a temperature of approximately 25 °C by re-circulation through a heat exchanger, with a whistle pump agitating and aerating the electrolyte. A constant capacitance condition was set, so as to achieve a current density of approximately 15 A dm^{-2} after the initial transitory regime. Coatings were grown for different

periods, giving a range of thickness. For both types of substrate, the coating growth rate was of the order of 1 µm min^{-1}. The samples were removed from the resin mould by dissolving the latter in acetone. It did not appear that any noticeable plastic deformation occurred during handling of the samples.

2.2. Coating thickness and microstructure

Coating thicknesses were measured with an Eban 2000 eddy current thickness gauge. This was cross-checked, and the thickness of the residual substrate was obtained, via SEM microscopy of polished cross-sections.

2.3. Curvature measurement

Residual stress in coatings formed on such thin strips will tend to give rise to curvature, which can be measured in order to obtain information about stress levels. It can be seen in Fig. 1, which shows photographs of untreated substrates and several coated samples in each case, that such curvature was quite noticeable and became more pronounced as the coating thickness was increased, as expected. It can also be seen that the coated beams were convex on the coated side, indicating that the coatings are under compressive residual stress.

Curvatures were measured using a scanning laser extensometer to obtain specimen height as a function of horizontal position, for samples supported at their ends on a flat surface. The resolution of the laser extensometer is a few microns and specimen self-weight has a negligible effect in this configuration. However, the surface roughness of these samples, and the scope for slight sample distortion (eg twisting), are such that the accuracy of these measurements is probably no better than about ± 50 µm. Nevertheless, with height changes of the order of 1–3 mm, and a large number of measurements being made over a horizontal distance of around 80 mm, it was possible to quantify the specimen shape, and hence obtain an average curvature, quite accurately.
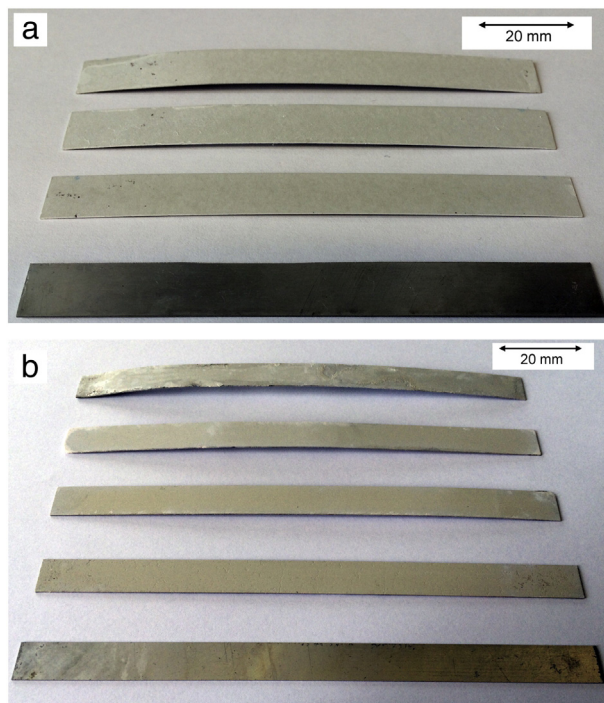

Fig. 1. Photographs of (a) an uncoated and 3 coated samples (60, 120 and 150 min) for Al-6082 substrates and (b) an uncoated and 4 coated samples (15, 30, 45 and 60 min) for Mg-AZ31 substrates.

Table 1
Data relating to measurement of the stiffness of PEO coatings on Al (6082) and Mg (AZ31) alloy substrates, obtained using 4-point bend testing of samples coated on both sides.

Coating thickness h (μm)	Substrate thickness H (μm)	Substrate alloy type	Sample width b (mm)	Sample length L (mm)	Load point spacing a (mm)	Peak load P (N)	Peak δ (μm)	Coating stiffness E_d (GPa)
92	225	Al-6082	10	90	40.1	0.098	104	46.0
143	231	Mg-AZ31	10	90	40.1	0.098	612	45.9

2.4. Stiffness values

In order to make deductions concerning residual stress levels for PEO coating systems, it is important to have at least reasonably accurate stiffness values for both coating and substrate (see Section 3 for details about this requirement). (Poisson ratio values are also needed, but these are less critical and are in general less sensitive to microstructural features such as microcracks.) For the substrates (well-known Al and Mg alloys), it is acceptable to take a handbook value for the Young's modulus (~68 and 45 GPa, respectively), but the stiffness of the PEO coating is sensitive to the architecture of the dense network of porosity and microcracks within it, which certainly has the effect of reducing the value well below that of the fully dense oxides (often by a factor of 5 or more).

The global in-plane Young's modulus of coatings was measured via symmetrical 4-point bending of sandwich bi-material beams, consisting of relatively thick (~100 μm) PEO coatings on both sides of relatively thin (~300–500 μm) substrates. Dead-weight loads were applied incrementally, and displacements were measured using a scanning laser extensometer. Elastic behaviour was confirmed by checking that load-deflection plots were linear and reversible. The following standard expression gives the central deflection, δ, exhibited by a beam with outer loading points a distance L apart, and inner loading points ($L - 2a$) apart, when subjected to a total load of $2P$:

$$\delta = \frac{Pa}{24(E_sI_s + E_dI_d)}\left(3L^2 - 4a^2\right) \tag{1}$$

where E_d, E_s are the Young's moduli of coating and substrate respectively and the corresponding second moments of area (about the neutral axis at the mid-plane) are given by

$$I_s = \frac{bH^3}{12} \text{ and } I_d = \frac{b}{12}\left((H + 2h)^3 - H^3\right) \tag{2}$$

in which b is the beam width, H is the substrate thickness and h is the thickness of the coatings (on each side).

The outcome of the coating stiffness measurement operations is shown in Table 1, where measured parameters and deduced Young's moduli values are shown for both types of coating. It can be seen that both coatings had an apparent stiffness of about 45 GPa. It should be recognised that these figures are only approximate. The value obtained is quite sensitive to the coating and residual substrate thicknesses and these do exhibit some local variations. Moreover, the stiffness of PEO coatings is expected to be sensitive to the presence of local defects such as microcracks, and the incidence of these is in turn likely to be sensitive to processing conditions. However, the values are at least broadly consistent with most previous measurements: they represent about 15% and 18% of the stiffness of the corresponding (fully dense) oxides.

3. Obtaining residual stress characteristics from curvature data

There has been extensive previous work on the relationships between stress levels in coatings and associated sample curvatures. In
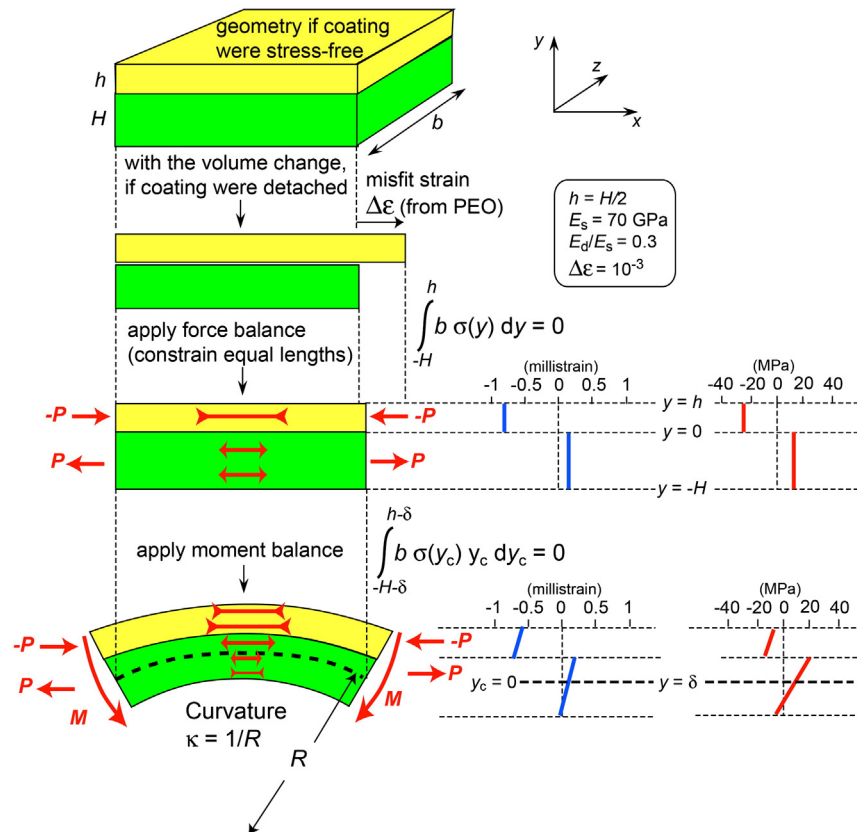

Fig. 2. Schematic of curvature creation from a misfit strain, with the stress and strain distributions shown corresponding to the listed conditions.

many cases, the coatings concerned are relatively stiff and contain high stress levels. Under such circumstances, measurable curvatures arise even when the ratio of coating thickness (h) to substrate thickness (H) is small. Furthermore, in many such cases, the surfaces concerned are very smooth and uniform, facilitating the accurate measurement of these curvatures (using optical reflection techniques). Under such circumstances (with $h \ll H$), the Stoney equation [22] can reliably be employed. For the equal biaxial case, as here, this can be written

$$\kappa = \frac{6h(1-\nu_s)}{E_s H^2}\sigma_d \tag{3}$$

where κ is the curvature, E_s and ν_s are, respectively, the Young's modulus and Poisson ratio of the substrate and σ_d is the stress in the coating ("deposit"). For a "Stoney limit" case, it is acceptable to identify a single stress level, since only the coating is under stress and the adoption of curvature has a negligible effect on the stress level and does not introduce any significant changes to it in the through-thickness direction.

The situation with PEO coatings, however, is very different from such cases. They do not have smooth surfaces, making highly accurate measurement (using optical reflection methods) difficult. Furthermore, they have relatively low stiffness, which tends to limit the magnitude of stress levels. Moreover, the PEO process involves continual restructuring throughout the coating thickness (via the plasma discharges), which relieves stresses and contributes substantially to their final level being relatively low. Under such circumstances, it is only by ensuring that

the coating thickness is relatively large compared to the substrate thickness (i.e., the $h \ll H$ condition is not satisfied) that curvatures large enough for suitably accurate measurement can be obtained. This is the case here, with h values of up to about $H/2$.

Fortunately, such cases can be analysed, although the complexity level is higher than for the Stoney treatment [23–26]. Since there are now significant stress levels in both constituents, and also significant through-thickness gradients in these as a result of curvature adoption, it is preferable to characterise the mechanism of stress creation via a misfit strain ($\Delta\varepsilon$) rather than as a stress level. The relationship between misfit strain and resultant curvature can be written [24]

$$\kappa = \frac{6E_d E_s(h+H)\ h\ H\ \Delta\varepsilon}{E_d^2 h^4 + 4E_d E_s h^3 H + 6E_d E_s h^2 H^2 + 4E_d E_s h\ H^3 + E_s^2 H^4} \tag{4}$$

where E_s and E_d are, respectively, the Young's moduli of substrate and coating and, for an equal biaxial case such as here, these should have their "biaxial" values ($E' = E / (1 - \nu)$). The behaviour exhibited by such a "non-Stoney" system is illustrated in Fig. 2, where a case is depicted in which $h \approx H/2$, and the coating stiffness is about a third that of the substrate, corresponds very approximately to a situation representative of the systems being examined here. Once a curvature has been measured, and the elastic constants and thicknesses of both constituents are known, then the value of the misfit strain can be obtained from Eq. (4), which reduces to the Stoney equation when $h \ll H$.

The misfit strain is the fundamental parameter characterising stress generation during a process (including any subsequent changes that
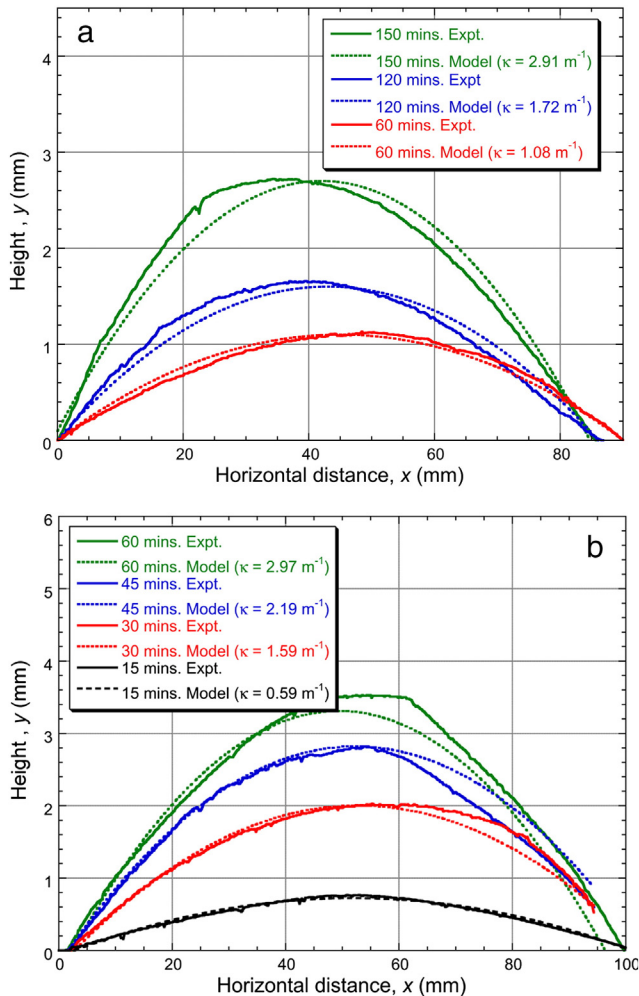

Fig. 3. Experimental and modelled shapes of the coated samples for (a) Al-based and (b) Mg-based substrates.
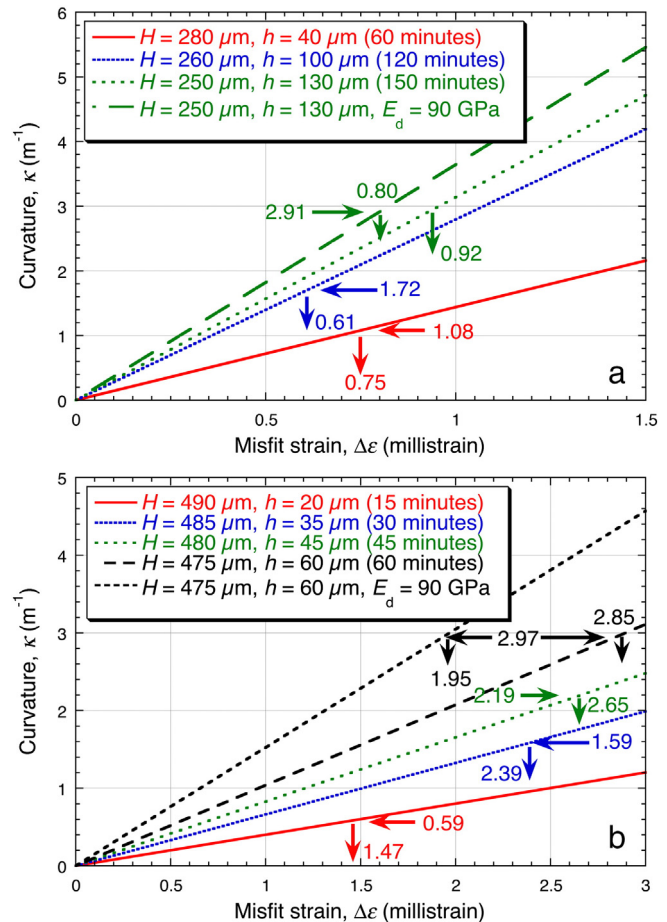

Fig. 4. Plots of curvature against misfit strain (from Eq. (4)), obtained using appropriate data for coating thickness and stiffness, showing derived values of the misfit strain for (a) Al-based substrates and (b) Mg-based substrates. Also shown, for the thickest coating case, is an indication of how the inferred misfit strain value would differ if the coating stiffness value used had been higher (50 GPa, rather than 25 GPa).

Table 2
Data relating to measurement of curvature and subsequent deduction of the misfit strain for PEO coatings on Al-6082 alloy substrates.

Process time t (min)	Coating thickness h (μm)	Substrate thickness H (μm)	Curvature κ (m^{-1})	Substrate (biaxial) modulus E'_s (GPa)	Coating (biaxial) modulus E'_d (GPa)	Misfit strain $\Delta\varepsilon$ (millistrain)
60	40	280	1.08	68/0.7 = 97	46/0.8 = 57.5	0.75
120	100	260	1.72	68/0.7 = 97	46/0.8 = 57.5	0.61
150	130	250	2.91	68/0.7 = 97	46/0.8 = 57.5	0.92

would give rise to stress, such as differential thermal expansion or contraction). In many practical situations, the substrate will be much thicker and/or stiffer than the coating, in which case the stress in the latter will be uniform and given by the product of the misfit strain and the (biaxial) coating modulus.

It may also be noted at this point that an assumption is being made here that, for a given type of coating, the misfit strain is uniform and independent of coating thickness. Under some circumstances, a misfit strain may change (slightly) as the process concerned progresses—for example because of changes in deposition conditions as successive layers are formed. However, since the PEO process is reconstructive— i.e., the whole coating is being regenerated in a similar way as it gets thicker—it seems appropriate for it to be ascribed a single value throughout its thickness.

4. Misfit strains and residual stress levels

4.1. Curvature evaluation

The data relating to curvature measurement are shown in Fig. 3, which gives measured and modelled profiles of several coatings for each type of alloy. The modelled plots were obtained by iterative adjustment of the parameters in the equation for a circle (coordinates of the centre and radius, R) until a best-fit profile was obtained: these are the shown in the figure, together with the corresponding curvature ($\kappa = 1/R$) values. The same operation was also carried out by fitting of the shape to a second order polynomial function and taking the second derivative of that expression as the curvature required. This is quicker and gave very similar values for κ to the first method.

4.2. Deduction of misfit strains

Using the obtained coating stiffness values (i.e., ~45 GPa for both Al- and Mg-based systems), the measured curvatures can be converted to misfit strains (using Eq. (4)). This operation is illustrated in Fig. 4, where it can be seen that the data for the three Al-based cases all imply a misfit strain value of around 0.6–0.9 millistrain. The data used in obtaining these values are presented in Table 2, with Poisson ratio values of 0.3 and 0.2 being used for substrate and coating respectively. The value of $\Delta\varepsilon$ has a positive sign—i.e., the stress-free length of the coating is greater than that of the substrate, as in the depiction in Fig. 3. For the Mg-based substrates, there is also a large degree of consistency, but with a larger value of around 2–3 millistrain (apart from that for the thinnest coating, which is a little lower.) The data for this system are shown in Table 3.

This sign of the misfit strain could be regarded as predictable (since the coating is often expected to occupy more volume than the substrate

it replaced), but it is not really possible to relate the magnitude of $\Delta\varepsilon$ to any physical characteristics. For example, the Pilling-Bedworth ratio (ratio of the volume of the unit cell of the oxide to that of the corresponding metal) is about 1.28 for alumina and 0.81 for magnesia. This could be taken to imply that the (linear) misfit should be positive with a magnitude of about 0.09 (90 millistrain) for alumina. For magnesia, on the other hand, it is negative (with a magnitude of about 60 millistrain). It is clear that such estimates bear no relation whatsoever to the measured values. In fact, it becomes clear that they are virtually meaningless when consideration is given to how the oxide actually forms during the PEO process, which involves the creation of deep, high temperature plasma channels through to the substrate, combination of the metal with oxygen in the vapour phase and melting of surrounding regions, followed by rapid condensation and solidification, and the creation of porosity and micro-cracks. Furthermore, even if this process does have a characteristic volume change, the associated stress (and the final misfit strain) would tend to be relaxed by subsequent discharges occurring through the same region. In practice, it is probably best to just accept the measured $\Delta\varepsilon$ as an experimental outcome.

Also shown in Fig. 4 is an indication of the sensitivity of the inferred misfit strains to the stiffness of the coating. It can be seen that doubling the Young's modulus from ~45 GPa to 90 GPa leads to a decrease in the misfit strain, from 0.92 to 0.80 millistrain for Al and from 2.85 to 1.95 millistrain for Mg. The resultant stress level (given, for a thin coating on a thick substrate, by the product of stiffness and misfit strain) is therefore raised by such doubling, but the increase is only by about 74% for Al and by about 37% for Mg (see Section 4.3).

4.3. Residual stress levels

Once the misfit strain associated with the transformation has been established, the corresponding stress level (or, if the coating is relatively thick, range of stress levels) can readily be established. (For a thin coating, it is simply given by the product of the misfit strain and the biaxial modulus of the coating.) This is illustrated in Fig. 5, which shows the stresses in the coating as a function of h/H, for relevant values of $\Delta\varepsilon$ and using the appropriate elastic constant values for the two cases. These curves were obtained from the following expressions [24] for the stresses in the coating at the free surface and at the interface.

$$\sigma_d\big|_{y=h} = \frac{-P}{b\,h} + E_d\,\kappa(h-\delta) \tag{5}$$

$$\sigma_d\big|_{y=h} = \frac{-P}{b\,h} - E_d\,\kappa\,\delta \tag{6}$$

Table 3
Data relating to measurement of curvature and subsequent deduction of the misfit strain for PEO coatings on Mg-AZ31 alloy substrates.

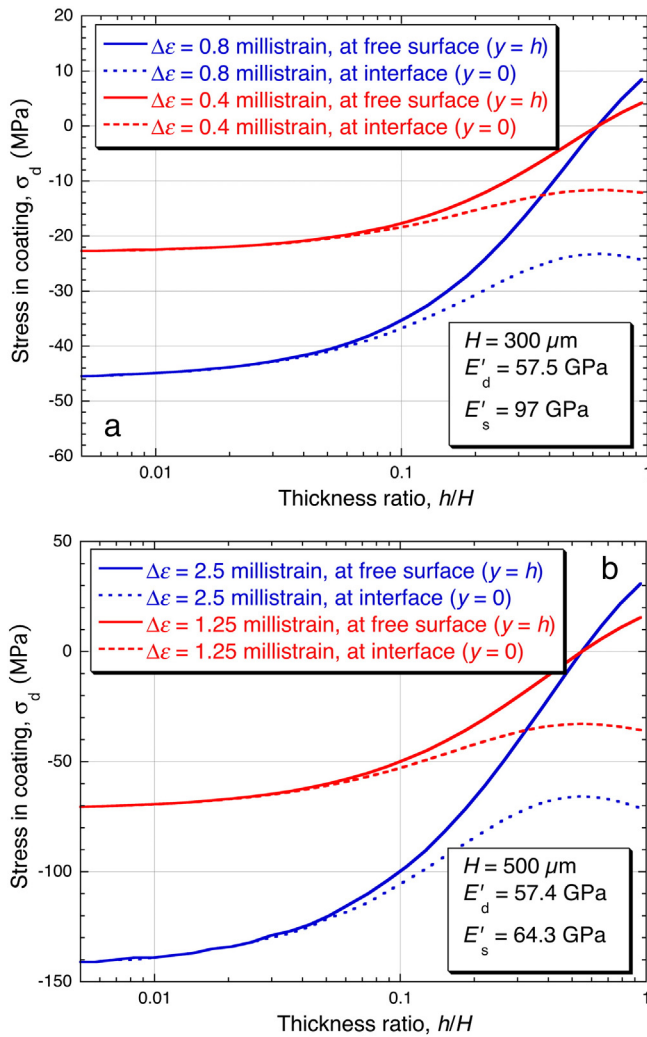| Process time t (min)	Coating thickness h (μm)	Substrate thickness H (μm)	Curvature κ (m^{-1})	Substrate (biaxial) modulus E'_s (GPa)	Coating (biaxial) modulus E'_d (GPa)	Misfit strain $\Delta\varepsilon$ (millistrain)
15	20	490	0.59	45/0.7 = 64.3	45.9/0.8 = 57.4	1.47
30	35	485	1.59	45/0.7 = 64.3	45.9/0.8 = 57.4	2.39
45	45	480	2.19	45/0.7 = 64.3	45.9/0.8 = 57.4	2.65
60	60	475	2.97	45/0.7 = 64.3	45.9/0.8 = 57.4	2.85

Fig. 5. Predicted stresses (from Eqs. (5) and (6)) in the coating (at the free surface and at the coating/substrate interface), for two different misfit strains, as a function of the thickness ratio, showing plots for (a) Al-based and (b) Mg-based coatings. The substrate thickness and the (biaxial) modulus values are as indicated.

where δ, the distance from the neutral axis ($yc = 0$) to the interface ($y = 0$), is given by

$$\delta = \frac{h^2 E_d - H^2 E_s}{2(h E_d + H E_s)} \quad (7)$$

and the ratio of the force P to the width b (see Fig. 4) can be obtained from

$$\frac{P}{b} = \Delta\varepsilon\left(\frac{h E_d H E_s}{(h E_d + H E_s)}\right) \quad (8)$$

It can be seen in Fig. 5(a) that, for the Al-based system, a misfit strain of the magnitude obtained here (~0.8 millistrain) will give rise (on relatively thick substrates) to a (compressive) coating stress of around 45 MPa. For the Mg-based system (Fig. 5(b)), for which a higher misfit strain value (~2.5 millistrain) has been deduced, the stress level is higher (~140 MPa). These values would fall by a factor of two if the deduced misfit strain were halved (while retaining the same elastic constants), as shown in Fig. 5. As mentioned above, however, there is an inter-dependence between curvature, misfit strain and coating stiffness, such that doubling the stiffness value used would, for a given (measured) curvature, only raise the deduced stress level by about 74% for Al (to ~70 MPa) or by about 37% for Mg (to ~190 MPa).

Values of this approximate magnitude (i.e., several tens of MPa) are significantly smaller than at least most of the values obtained previously by X-ray diffraction. However, as mentioned in the introduction, care must be taken with XRD data relating to lattice strains in PEO coatings. It is worth noting that there are reasons related to the nature of the PEO process for expecting the true value to be relatively low. On the other hand, the values obtained here are appreciably larger than those from the previous study based on curvature measurement [21]. In any event, the stress levels reported here should be regarded as approximate, particularly since the coating stiffness has not been established to very high precision (and indeed it probably varies between PEO coatings produced under different conditions). Nevertheless, measuring the stiffness of these coatings, even without high precision, is clearly preferable to assuming the handbook (fully dense) value for the oxide concerned.

The broad conclusion from the current work—i.e., that the PEO process gives rise to significant, but relatively low, compressive coating stresses (of the order of several tens of MPa)—is fairly well defined. Moreover, it does appear that the misfit strain and hence the residual stress level are somewhat higher for Mg-based systems than for those on Al substrates. It is difficult at this stage to speculate on explanations for this difference, although it is certainly worth noting that PEO is a highly complex process, with several factors expected to affect the misfit strain. A number of these, such as oxide electrical and thermal properties, are likely to differ significantly between types of metal substrate.

4.4. Likelihood of coating spallation

The level of residual stress in a coating is of interest for several reasons. One of these is that the associated stored elastic strain energy represents a driving force for spallation since it is likely that at least most of this energy would be released if interfacial debonding were to occur. This effect has been studied in some detail [24,27] and of course it is relevant, not only to possible spallation of coatings but also to issues like experimental measurement of interfacial toughness [28,29].

For a uniform (biaxial) misfit strain, and a thin (Stoney case) coating (relative to the substrate), the strain energy release rate (in J m⁻²) for interfacial debonding can be written as

$$G_i = 2\left(\frac{\frac{1}{2}\text{stress} \times \text{strain} \times \text{volume}}{\text{area}}\right) = \sigma_d\left(\frac{\sigma_d}{E_d'}\right)\left(\frac{hA}{A}\right) = \frac{\sigma_d^2}{E_d'}h \quad (9)$$

based on the assumption that all of the stress is relaxed on debonding; hence, the factor of 2 accounts for both sets of in-plane stresses. Of course, the sign of the stress makes no difference to this calculation,
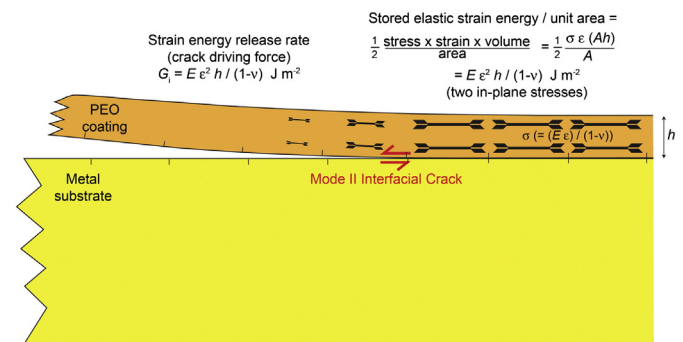

Fig. 6. Schematic depiction of the spallation of a PEO coating as a result of the release of elastic strain energy associated with (equal biaxial, compressive) residual stresses in it. The reference lines across the interface indicate how shear will be generated there as the stresses become relaxed during debonding, driving the interfacial crack under mode II conditions.
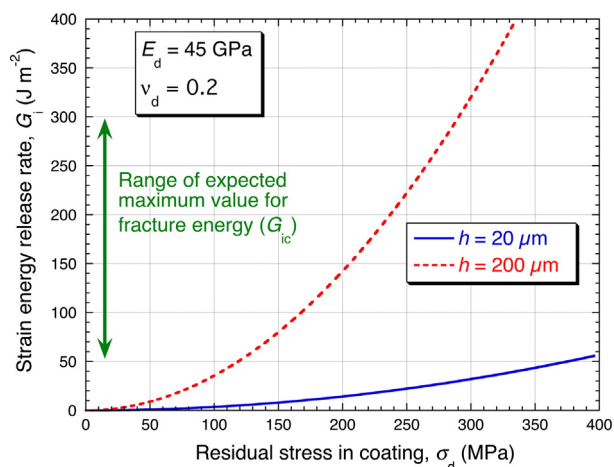
Fig. 7. Plot of interfacial strain energy release rate values (obtained using Eq. (9)), as a function of the stress level in the coating, for two coating thicknesses.

since the stored elastic strain energy (for a given stress magnitude) is the same whether it is compressive or tensile, and this is reflected in the fact that it is proportional to the square of the stress. This is a very simple fracture mechanics situation, with no dependence on the crack length (since, for an incremental crack advance, the volume of material in which strain energy gets released is independent of crack length). This type of spallation process is illustrated in Fig. 6, where it can be seen that propagation of the interfacial crack occurs under mode II (shearing) conditions. Comparing the magnitude of G_i with the corresponding critical value, i.e., the fracture energy of the interface, allows prediction of whether debonding is energetically favoured (leaving aside issues relating to initiation of the interfacial crack).

A plot is shown in Fig. 7 of how G_i depends on the level of stress in a (PEO) coating, for two coating thicknesses. Of course, the interfacial fracture energy, G_{ic}, is in general unknown, and it is possible that it is relatively high. However, the fracture energy of PEO coatings themselves is unlikely to be greater than a couple of hundred J m^{-2} or so and a crack could run through the coating close to the interface, where the driving force would be similar to that for interfacial cracking. It can be seen from Fig. 7 that, while the (common) observation that PEO coatings of up to about 200 μm in thickness do not readily undergo (spontaneous) spallation is consistent with the stress levels within them being of the order of several tens of MPa, or even 200 MPa, it would be difficult to explain if their magnitude were substantially greater than this (i.e., several hundreds of MPa).

5. Conclusions

The following conclusions can be drawn from this work.

(a) Curvatures in the approximate range of 1–3 m^{-1} (i.e., radii of curvature between about 1 m and 300 mm) were measured for three thin strip samples of Al alloy with different PEO coating thicknesses and for four similar samples of Mg alloy. Using measured thicknesses and elastic constants, these curvatures were found to correspond to misfit strains of about 0.6–0.9 millistrain for Al and around 2–3 millistrain for Mg. These values are considered to be broadly characteristic of the PEO transformations concerned (i.e., conversion of Al to alumina, or Mg to magnesia, via a series of electrical discharges).

(b) Such a misfit strain can be converted to a through-thickness distribution of residual stress for any given sample geometry and dimensions, using elastic constants of the coating and substrate. In the case of a (planar) substrate that is considerably thicker than the coating, there will just be a (uniform) stress in the coating, at a level given by the product of the misfit strain and the

(biaxial) modulus of the coating. For the biaxial modulus value used in the present work (~50–60 GPa in both cases), this stress is compressive, with a magnitude of ~40–50 MPa for Al and 130–150 MPa for Mg.

(c) Such stress levels are somewhat lower than those reported in most previous studies based on the shift of X-ray diffraction peaks from the crystalline (alumina) phases present in the PEO. However, such measurements need to be carefully interpreted for PEO coatings, and account taken of their (relatively low) global stiffnesses. Outcomes from XRD studies can probably be reconciled with that from the present work in terms of this stiffness issue and the range of local lattice strains that may arise in PEO coatings. On the other hand, the values reported here are larger in magnitude than those from the single previous study based on curvature measurements, which led to deduced stresses of the order of 10 MPa (compressive).

(d) A brief (theoretical) study has also been made of the strain energy release rate (driving force for spallation) associated with PEO coatings in typical thickness ranges, as a function of the residual stress level. It is concluded that, while the observed (high) resistance of PEO coatings to spallation is consistent with the (relatively low) stress levels measured in the current study, this would not be expected if these stresses were substantially higher.

Acknowledgements

References

[1] X. Nie, A. Leyland, H.W. Song, A.L. Yerokhin, S.J. Dowey, A. Matthews, Surf. Coat. Technol. 116–119 (1999) 1055–1060.
[2] S.V. Gnedenkov, O.A. Khrisanfova, A.G. Zavidnaya, S.L. Sinebrukhov, P.S. Gordienko, S. Iwatsubo, A. Matsui, Surf. Coat. Technol. 145 (2001) 146–151.
[3] J.A. Curran, T.W. Clyne, Surf. Coat. Technol. 199 (2005) 168–176.
[4] R.H.U. Khan, A. Yerokhin, X. Li, H. Dong, A. Matthews, Surf. Coat. Technol. 205 (2010) 1679–1688.
[5] F. Monfort, A. Berkani, E. Matykina, P. Skeldon, G.E. Thompson, H. Habazaki, K. Shimizu, Corros. Sci. 49 (2007) 672–693.
[6] Y.J. Guan, Y. Xia, Trans. Nonferrous Metals Soc. China 16 (2006) 1097–1102.
[7] H. Kalkanci, S.C. Kurnaz, Surf. Coat. Technol. 203 (2008) 15–22.
[8] X. Zhang, Y. Zhang, L. Chang, Z. Jiang, Z. Yao, X. Liu, Mater. Chem. Phys. 132 (2012) 909–915.
[9] R.F. Zhang, S.F. Zhang, J.H. Xiang, L.H. Zhang, Y.Q. Zhang, S.B. Guo, Surf. Coat. Technol. 206 (2012) 5072–5079.
[10] R.O. Hussein, X. Nie, D.O. Northwood, Surf. Coat. Technol. 205 (2010) 1659–1667.
[11] Y.J. Guan, Y. Xia, G. Li, Surf. Coat. Technol. 202 (2008) 4602–4612.
[12] G. Sundararajan, L. Rama Krishna, Surf. Coat. Technol. 167 (2003) 269–277.
[13] Z.Q. Wu, Y. Xia, G. Li, F.T. Xu, Acta Metall. Sin. 44 (2008) 119–124.
[14] Z.T. Chen, G.A. Li, Z.Q. Wu, Y.A. Xia, Math. Sci. Eng. A 528 (2011) 1409–1414.
[15] Y.J. Guan, Y. Xia, F.T. Xu, Surf. Coat. Technol. 202 (2008) 4204–4209.
[16] D. Asquith, A. Yerokhin, N. James, J. Yates, A. Matthews, Metall. Mater. Trans. 44A (2013) 4461–4465.
[17] R.H.U. Khan, A.L. Yerokhin, A. Pilkington, A. Leyland, A. Matthews, Surf. Coat. Technol. 200 (2005) 1580–1586.
[18] D. Shen, J. Cai, C. Guo, P. Liu, Chin. J. Mech. Eng. 26 (2013) 1149–1153.
[19] R.H.U. Khan, A.L. Yerokhin, A. Matthews, Philos. Mag. 88 (2008) 795–807.
[20] Y. Gu, C. Chen, S. Bandopadhyay, C. Ning, Y. Guo, Surf. Eng. 28 (2012) 498–502.
[21] Y. Kuznetsov, A. Kossenko, B. Kazansky, *Israeli-Russian Bi-National Workshop (XII)*. 2013. Jerusalem, 2013, pp. 108–116.
[22] G.C.A.M. Janssen, M.M. Abdalla, Fv Keulen, B.R. Pujada, Bv Venrooy, Thin Solid Films 517 (2009) 1858–1867.
[23] L.B. Freund, J.A. Floro, E. Chason, Appl. Phys. Lett. 74 (1987) 1987–1989.
[24] T.W. Clyne, Key Eng. Mater. 116 (7) (1996) 307–330.
[25] Y.C. Tsui, T.W. Clyne, Thin Solid Films 306 (1997) 23–33.
[26] T.W. Clyne, in: K.H.J. Buschow, R.W. Cahn, M.C. Flemings, B. Ilschner, E.J. Kramer, S. Mahajan (Eds.), Elsevier, Oxford, 2001, pp. 8126–8134.
[27] T.W. Clyne, S.C. Gill, J. Therm. Spray Technol. 5 (1996) 1–18.
[28] P.G. Charalambides, H.C. Cao, J. Lund, A.G. Evans, Mech. Mater. 8 (1990) 269–283.
[29] S.J. Howard, Y.C. Tsui, T.W. Clyne, Acta Metall. Mater. 42 (1994) 2823–2836.